ACS Photonics

Article

pubs.acs.org/journal/apchd5

Plasmon–Exciton Interactions in a Core–Shell Geometry: From Enhanced Absorption to Strong Coupling

Tomasz J. Antosiewicz,*[,†,‡] S. Peter Apell,[‡] and Timur Shegai*[,‡]

[†]Centre of New Technologies, University of Warsaw, Żwirki i Wigury 93, 02-089 Warsaw, Poland

[‡]Department of Applied Physics, Chalmers University of Technology, SE-412 96 Göteborg, Sweden

Supporting Information

ABSTRACT: We present a detailed Mie theory, finite-difference time-domain, and quasi-static study of plasmon–exciton interactions in a spherical core–shell geometry. In particular, we report absorption, scattering, and extinction cross sections of a hybrid core–shell system and identify several important interaction regimes that are determined by the electromagnetic field enhancement and the oscillator strength of electronic excitations. We assign these regimes to enhanced-absorption, exciton-induced transparency and strong coupling, depending on the nature of the observed spectra of the coupled plasmon–exciton resonances. We also show the relevance of performing single-particle absorption or extinction measurements in addition to scattering to validate the interaction regime. Furthermore, at relatively high, yet realistic oscillator strengths we observe emergence of a third mode, which is not predicted by a classical coupled harmonic oscillator model and is attributed to the geometrical resonance of the structure as a whole.

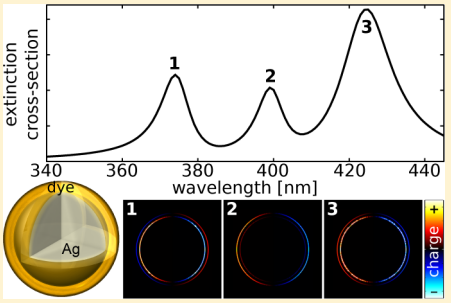

KEYWORDS: *plexciton, strong coupling, surface plasmon, molecular exciton*

Interaction of localized surface plasmons in metallic nanostructures and electronic excitations in quantum-sized objects such as organic chromophores or quantum dots has been a subject of intense research on both the theoretical[1−7] and experimental[8−25] level recently. This is in part motivated by similarities between these plasmon–exciton systems and atomic, photonic, and quantum optics systems for which truly quantum effects such as electromagnetically induced transparency (EIT), cavity quantum electrodynamics, and photon blockade have been reported.[26−28] The hope is that these exotic quantum effects may be observed in hybrid plasmon–exciton structures at relatively nondemanding experimental conditions such as room temperature, atmospheric pressure, and a large number of chromophore molecules due to the fact that plasmons are inherently fast and allow focusing of electromagnetic modes into deep subwavelength volumes. On the other hand, many reported plasmon–exciton systems are topologically similar to various surface-enhanced Raman, infrared absorption, and enhanced-fluorescence structures studied previously.[29−37] These similarities further motivate studies of plasmon–exciton interactions in relation to light harvesting,[38,39] sensing,[40] ultrafast dynamics, and nonlinear effects.[24,41] Strikingly, interactions between plasmons and excitons can be described rather well by a purely classical coupled harmonic oscillator model and indeed were demonstrated to show EIT-like or even strong coupling behavior.[2] Despite very intense research, however, there still remain several points to be clarified. These include, for example, confident assignment of interaction regimes based on comparison between scattering and absorption cross sections and mode anticrossing.

Here, we perform theoretical analysis of spherical core–shell nanostructures using Mie theory, the finite-difference time-domain (FDTD) method, and the quasi-static approximation as a function of geometrical parameters of the system, oscillator strength of the absorbing medium, and line width of electronic excitations. In particular, we show that these structures can be found in several distinct interaction regimes ranging from enhanced absorption to strong coupling depending on the exact conditions. By investigating very large dye permittivities, which can be found experimentally in molecular J-aggregates that have very high oscillator strength or at low temperatures where the exciton line width becomes very narrow, we demonstrate emergence of three peaks in both absorption and scattering, a scenario strongly deviating from a coupled-oscillator model. To our knowledge, there have been only a few examples where this kind of behavior was reported.[6]

This paper is structured as follows. We begin by introducing the employed methodology, focusing in particular on the Lorentzian permittivity of a model dye and sketching a brief quasi-static analysis of the optical properties of a plexciton in a core–shell nanostructure. Next, we show how the size of a metal core affects the optical properties of the nanostructure and discuss it in the context of absorption in constituent elements, separately in the core and in the shell. Subsequently, we demonstrate how coupling depends on the strength of the

Received: January 24, 2014
Published: April 14, 2014

dye resonance and that for large oscillator strengths the core−shell geometry is characterized by a three-peaked spectrum. Finally, we discuss consequences of interband absorption in the metal on the optical spectra of strongly coupled nanostructures.

THEORETICAL CONSIDERATIONS

As depicted in Figure 1a, we consider a layered sphere with a core radius of r and a shell of thickness h immersed in a

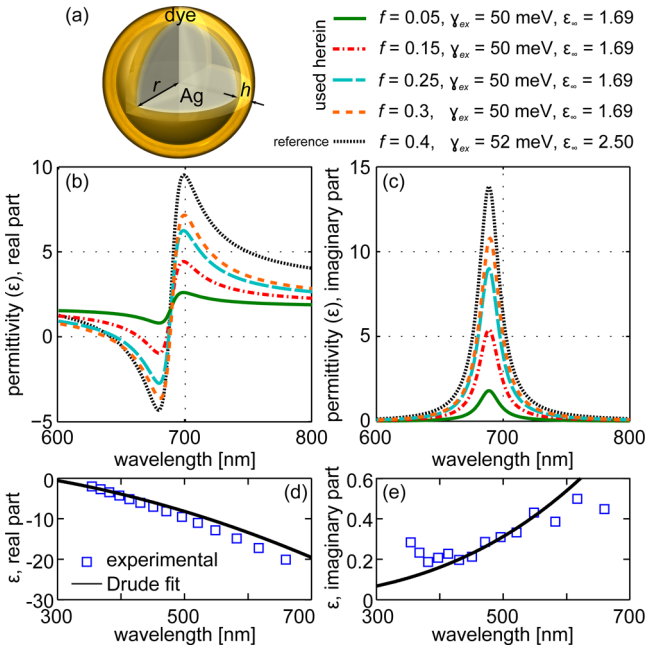

Figure 1. (a) Core−shell nanoparticle used to study plasmon−exciton coupling: silver core radius r and dye shell thickness h. (b) Real and (c) imaginary parts of permittivities of dye layers centered at ∼1.8 eV with oscillator strength f, damping γ_{ex}, and background permittivity ε_∞. The first four curves show permittivities used in this work. The black dotted line shows for comparison the permittivity used to model the optical properties of J-aggregates in a poly(vinyl alcohol) solution.[23] (d) Real and (e) imaginary parts of silver measured by Johnson and Christy[42] (squares) and the Drude fit used here (line).

medium with a refractive index of 1.3. The core is made from silver described by the Drude model, $\varepsilon_c(\omega) = \varepsilon_p - \omega_p^2/(\omega(\omega + i\gamma))$, neglecting any interband absorption at short wavelengths. The parameters are calculated by fitting measurements obtained by Johnson and Christy[42] in the 400−600 nm range (note the spectral position of the plasmon resonances in subsequent figures) and are $\varepsilon_p = 3.7$, $\hbar\omega_p = 8.55$ eV, and $\hbar\gamma = 65$ meV (see Figure 1d,e).[43]

The permittivity of the dye layer is modeled using a single Lorentzian function in terms of a dimensionless oscillator strength f, a resonance width γ_{ex}, and its position ω_{ex} and is modified by the large-frequency permittivity ε_∞ according to

$$\varepsilon_{ex}(\omega) = \varepsilon_\infty + \frac{f\omega_{ex}^2}{\omega_{ex}^2 - \omega^2 - i\gamma_{ex}\omega} \quad (1)$$

At resonance ($\omega = \omega_{ex}$) the above equation simplifies to

$$\varepsilon_{ex}(\omega_{ex}) = \varepsilon_\infty + i\frac{f\omega_{ex}}{\gamma_{ex}} \quad (2)$$

Note that the imaginary part of the permittivity for a given oscillator strength depends on the resonance frequency, leading to a change in permittivity when the resonance of the exciton changes. Thus, the permittivities depicted in Figure 1b,c are valid only for $\hbar\omega_{ex} = 1.8$ eV, and for calculations in which the dye resonance coincides with a variable resonance frequency of the metal core (variable r) this would lead to unwanted changes. Therefore, we recast the oscillator strength as $\tilde{f} \equiv f\Omega/\omega_{ex}$, where $\hbar\Omega = 1.8$ eV at which f is defined. This means that when we quote f values we refer directly to values shown in Figure 1, while the actual $\tilde{f}$ value used in the equations is the rescaled one. As a result, the span of the real and imaginary parts of the permittivity is preserved. The optical response of the metal−dye structure is strongly dependent on the permittivity of the dye; we thus restrict the possible values to be not larger than reported in recent literature, with a few exceptions to illustrate trends. The limiting reference permittivity we choose is reported for J-aggregates in a poly(vinyl alcohol) solution[23] (black dotted line in Figure 1b,c), and all dye material values are smaller (in terms of absolute values). This is especially important for the real part of the permittivity, since very large negative values over a broad wavelength range may turn the dye into a metal-like material.

Optical scattering and absorption calculations are performed using Mie theory for a coated sphere.[44] Additionally, we use the FDTD method to verify the accuracy of the implementation of the Mie code, to supplement the results with surface charge distributions, and perform additional simulations for non-spherical objects to help in explaining observed characteristics.

Quasi-static Analysis. Before presenting detailed Mie theory and FDTD calculations we briefly sketch an outline of expected results (for a detailed derivation, refer to the Supporting Information, SI). Bohren and Huffman give the expression for the quasi-static polarizability of a coated ellipsoid,[44] which serves as the basis of the current argument. In a simple case of a coated sphere when the geometrical factors L are the same and the ratio of the core volume to that of the total structure is s, the modes of the structure occur when the denominator of the polarizability becomes zero,

$$\varepsilon_{ex}(p + \varepsilon_c) + q(\varepsilon_c - \varepsilon_{ex})(1 - \varepsilon_{ex}) = 0 \quad (3)$$

where $p + 1 = L^{-1}$, we have introduced a coupling term $q \equiv (1 - s)(1 - L)$, and the permittivity of the surrounding medium is 1 (equivalent to measuring all ε in units of the outside permittivity). With $q = 0$, *i.e.*, no shell, there is only one real mode defined by the relation $p + \varepsilon_c = 0$. Solving this equation with a Drude permittivity yields the well-known resonance condition of a localized surface plasmon at $\omega_1 = \omega_p/(\varepsilon_p + p)^{1/2}$.

With q very small (thin shell limit) the second term in eq 3 is only a small correction, and we can write, remembering that $\varepsilon_c \approx -p$,

$$p + \varepsilon_c = q\frac{(\varepsilon_{ex} + p)(1 - \varepsilon_{ex})}{\varepsilon_{ex}}\Bigg|_{\omega_1} \quad (4)$$

We can now recast p as $p' = p + q(\varepsilon_{ex} + p)(\varepsilon_{ex} - 1)/\varepsilon_{ex}$ with the coupled resonance shifted to $\tilde{\omega}_1 = \omega_p/(\varepsilon_p + p')^{1/2}$.

Equation 3 can also become zero when $\varepsilon_{ex} \approx 0$ provided that its second term is indeed small; with a nonzero q this mode is no longer spurious. To solve this in a straightforward way, we first look for solutions of $\mathrm{Re}(\varepsilon_{ex}) = 0$, which are given by solving

dx.doi.org/10.1021/ph500032d | ACS Photonics 2014, 1, 454−463

$$\omega^4 + \omega^2\left[{\gamma_{ex}}^2 - {\omega_{ex}}^2\left(2 + \frac{f}{\varepsilon_\infty}\right)\right] + {\omega_{ex}}^4\left(1 + \frac{f}{\varepsilon_\infty}\right) = 0 \tag{5}$$

Depending on the discriminant, there may be no, one, or two solutions as defined by the relations between the constant term, the line width, and oscillator strength. When the discriminant Δ of eq 5 is zero, there is only one mode; however, also for $\Delta < 0$ a mode is present due to a nonzero γ_{ex}. Thus, in a coupled core−shell structure one finds two resonances, as was reported previously, even if the real part of ε_{ex} is larger than zero. Hence, we will not focus on these cases.

By choosing appropriate values for ε_∞, f, and γ_{ex} the discriminant can be made positive, and that leads to two solutions with positive frequencies (see SI for details). When neglecting losses ($\gamma_{ex} = 0$), they are

$$\omega_2 = \omega_{ex}\sqrt{1 + \frac{f}{\varepsilon_\infty}}, \qquad \omega_3 = \omega_{ex} \tag{6}$$

Coupling is introduced in a similar way as before by estimating the second term of eq 3 at $\omega_{2,3}$. This term enters via a rescaled exciton permittivity ε_∞, and the modes become

$$\tilde{\omega}_2 = \omega_{ex}\sqrt{1 + f\left(q\frac{\varepsilon_c}{\varepsilon_c + p}\bigg|_{\omega_2} + \varepsilon_\infty\right)^{-1}}, \qquad \tilde{\omega}_3 = \omega_{ex} \tag{7}$$

Thus, in the limit of negligible shell losses, one resonance undergoes shifting, while the other remains relatively stable at the exciton frequency.

The full spectrum of a core−shell structure may consist of up to three resonances that originate from a shifted plasmon resonance as well as up to two shifted shell resonances. Below, we shall use Mie theory and FDTD simulations to go though various examples of structures and illustrate a wide range of possible plasmon−exciton interaction results.

RESULTS AND DISCUSSION

Defining Three Coupling Regimes. The predominant experimental methods used to analyze the optical properties of coupled metal−dye composites are scattering measurements performed on single particles employing dark field microscopy. Single-particle measurements have the advantage of eliminating ensemble averaging and the resulting inhomogeneous broadening, giving usually a better signal. A drawback of dark field measurements is that obtaining extinction of a single particle, thus also absorption, is difficult. This is also the reason that many theoretical works also focus mainly on scattering. However, neglecting absorption means that a lot of information is not utilized, and we strive to remedy this.

In Figure 2a we present the scattering efficiency (all efficiencies are calculated as ratios of optical cross sections to geometrical cross sections) of a core−shell structure in which the radius of the metal core is varied from 10 to 50 nm. For each radius we first calculate the position of the extinction maximum and set the exciton resonance to that value with f = 0.05 and $\hbar\gamma_{ex}$ = 50 meV. The result is a two-peaked spectrum that blue-shifts with decreasing radii. The dip in between is indicative of coupling between the exciton in the shell and the plasmon of the core; however, the strength of this coupling varies and determines the regime. The coupling strength depends on a number of factors. Here, by changing the core

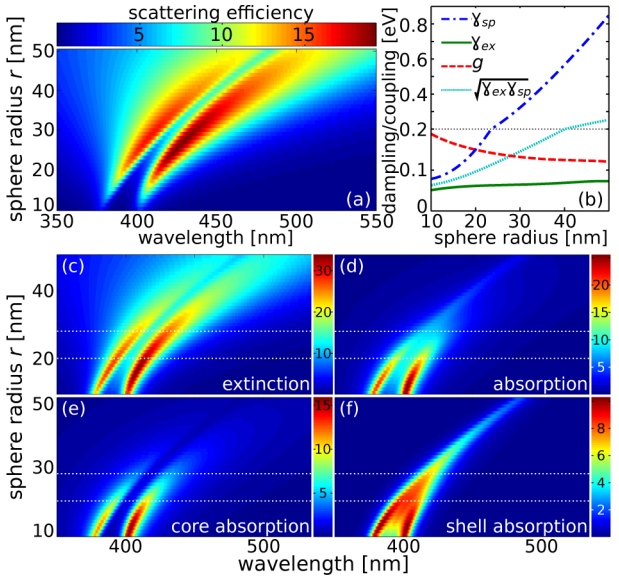

Figure 2. (a) Scattering efficiency of a core−shell nanoparticle−silver core with a variable r, h = 2 nm, f = 0.05, $\hbar\gamma_{ex}$ = 50 meV, and the exciton resonance set to the extinction maximum of a bare core of the same size made of silver. For small r the plasmon−exciton interaction gives a broad and deep scattering minimum. (b) Plasmon and exciton line widths, γ_{sp} and γ_{ex}, respectively, $(\gamma_{sp}\gamma_{ex})^{1/2}$, and the plasmon−exciton coupling rate g extracted from fitting a coupled harmonic oscillator model to scattering spectra shown in (a). Using the criterion $g > (\gamma_{sp}, \gamma_{ex})$ the system is strongly coupled for radii smaller than 20 nm, while for $g > (\gamma_{sp}\gamma_{ex})^{1/2}$ for $r < 28$ nm. Note that the y-scale is changed for dephasing rates larger than 0.2 eV (marked with a dotted line). (c) Extinction, (d) total absorption, (e) core absorption, and (f) shell absorption. The horizontal lines mark the strong coupling regime limiting radii obtained from (b). A dip in scattering, extinction, and core absorption is present in the whole considered range. Total and shell absorption have only one peak for $r > 30$ nm. Only for $r < 30$ nm (weak criterion) does the coupling begin to affect total absorption strongly, and for $r < 20$ nm (strong criterion) an absorption dip develops indicative of strong coupling.

diameter we vary two of them: the electric field enhancement near the core and the dye-to-metal volume ratio. The changes are correlated, and when the former value for r = 10 to 50 nm goes from ca. 30 to 3, it is accompanied by a volume ratio change from 0.7 to 0.1. Thus, the coupling strength decreases with an increasing radius.

We use a coupled harmonic oscillator model to calculate, based on Figure 2a, the coupling strength g as well as the line width for the plasmon resonance and the exciton.[2] The fitted values are shown in Figure 2b. The coupling strength g shown by the dashed red line is indeed a decreasing function of r. For all considered radii the fitted exciton dephasing rate γ_{ex} is smaller than g and almost constant, while the plasmon line width varies considerably. In the literature the relation for strong coupling between g and γ_{ex}, γ_{sp} has been given as $g > (\gamma_{ex}, \gamma_{sp})$ or $g > (\gamma_{ex}\gamma_{sp})^{1/2}$ (see, for example, ref 8). When the radius is large, the plasmon dephasing rate is much larger than the coupling strength and the system is in a weakly coupled state, also called energy transfer.[5] The weaker of the two conditions is fulfilled only for $r < 28$ nm, while the stronger for $r < 20$ nm. Thus, a question here arises: which of the two inequalities is required for strong coupling to be identified?

This ambiguity can be solved by considering complementary measurements of extinction and absorption, including deter-

dx.doi.org/10.1021/ph500032d | ACS Photonics 2014, 1, 454−463

mination in which part of the core−shell structure is energy in fact dissipated. These are gathered in Figure 2c−f. We have also indicated both critical radii to clearly mark the three regions with different relations between the dephasing parameters. While the scattering plot does not provide concise qualitative information, absorption does, especially when split between the core and shell contributions. As long as the sphere radius is greater than 30 nm, total absorption (Figure 2d) is characterized by a sharp peak over a much broader one. As r tends to 28 nm, the narrow peak broadens, and for r = 20 nm splits into two. The contribution from the core in Figure 2e, similar to scattering, has a two-peaked spectrum. However, the shell absorption spectrum (Figure 2f) is different. For r > 30 nm it has only one narrow peak, which for 20 < r < 30 nm undergoes broadening and finally splitting.

These clearly marked trends are exemplified in Figure 3, where we present cross sections for three representative cases with r = 45 nm in Figure 3a,b, 25 nm in Figure 3c,d, and 15 nm in Figure 3e,f. The left column shows extinction and scattering

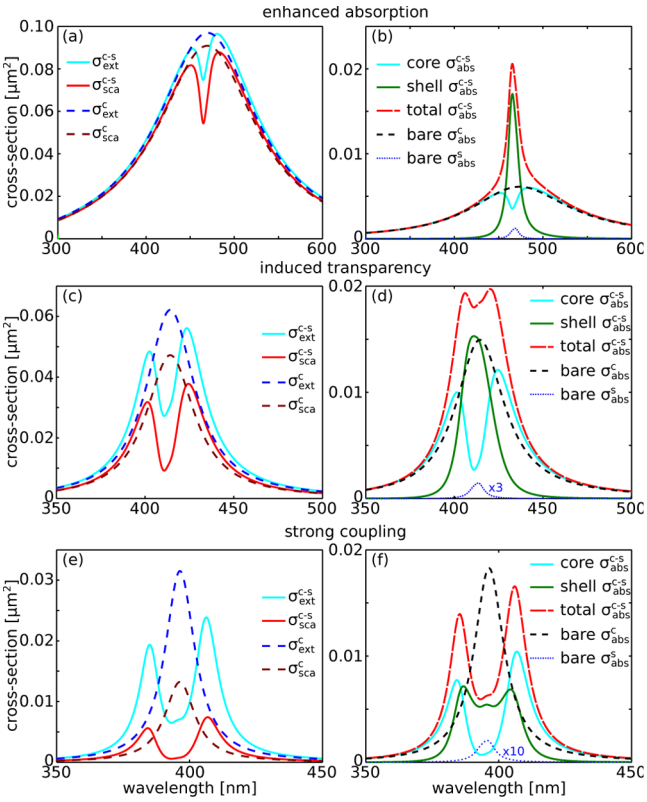

Figure 3. Optical cross sections of nanoparticles with silver cores having (a, b) r = 45 nm, (c, d) 25 nm, and (e, f) 15 nm and a dye shell 2 nm in thickness with f = 0.05, $\hbar\gamma_{ex}$ = 50 meV, and the exciton resonance coincides with the plasmon resonance for any given radius. (a, c, e) Comparison of extinction and scattering of core−shell "c-s" (continuous lines) and bare core "c" (dashed lines) structures. (b, d, f) Breakdown of absorption in the core−shell nanoparticle compared with that of a bare core and a bare shell "s" (dotted line). (a, b) Enhanced absorption: a very small extinction dip with an absorption peak compensating for reduced scattering. Absorption at resonance is increased 4-fold. (c, d) Induced transparency: scattering strongly reduced, absorption in the dye layer has one peak, but is now comparable to that of the core and bare core; total absorption shows a very weak dip. (e, f) Strong coupling: scattering is almost suppressed at the original resonance position. Both core- and shell-absorption exhibit peak splitting.

for a bare core (dashed lines) and a core−shell (solid lines) structure, while the right one compares core−shell total absorption with its two components and the bare absorption core spectrum. For r = 45 nm the dip in scattering is narrow and weak and is partly offset by an increase in absorption. This increased absorption is caused by the shell, which feels an enhanced electric field and contributes more than 80% of the absorption value at the peak position. Note that total absorption in the core−shell structure exceeds 4-fold the bare core value. This behavior is indicative of enhanced absorption, also called energy transfer.[5]

In the intermediate radius range, r = 25 nm, scattering is reduced at the dip to 20% of the bare core value and extinction to 50%. These considerable changes are now accompanied by (weak) peak splitting. While in principle strong coupling could be ascribed to this case, an analysis of the absorption spectrum indicates that this is not yet the case. At peak total absorption is only 30% larger than for the bare core, and additionally its spectrum is also slightly broader; however, most noteworthy are the beginnings of a dip. The core absorption (for the core−shell structure) exhibits a deep minimum at the exciton line, but at the same time the shell absorption exhibits a peak. The important difference between this case and the previous one is the fact that the shell absorption is equal to that of the bare core, so overall absorption remains small.

A further reduction in the particle radius to 15 nm is accompanied by strong splitting of approximately 30 nm (240 meV). This splitting is observed for both scattering and absorption, giving in total a deep extinction minimum at the exciton resonance. Interestingly, at the dip scattering is strongly suppressed and total absorption is dominant. The individual contributions to absorption are split unequally between core and shell (at the original resonance ω_{sp}), with both constituents exhibiting strong splitting. One difference is that core absorption is reduced drastically at the resonance due to coupling, while shell absorption remains relatively strong. Thus, we show that in a core−shell structure the strong coupling (vacuum Rabi splitting) is characterized by splitting, visible not only in the scattering spectrum but also in the absorption spectrum. While measuring absorption of a single particle is not easy, a measurement of a part of the extinction will indicate if the absorption peak is indeed split.[8] Otherwise, as for r = 25 nm, the state should rather be classified as induced transparency.

Large Oscillator Strengths. Up to this point we have only considered dye with an exciton line width of 50 meV and an oscillator strength of f = 0.05. As plotted in Figure 1 the permittivity range of the dye shell is moderate with the real part $\mathrm{Re}(\varepsilon) \in (0.8,2.6)$ and imaginary part $\mathrm{Im}(\varepsilon) \leq 1.8$. However, dyes with larger variations of an equivalent permittivity can be found with $\mathrm{Re}(\varepsilon) \in (-4,9)$ and $\mathrm{Im}(\varepsilon) \leq 14$ (ref 23). There are two ways of adjusting the permittivity: one being f and the other γ_{ex}. Here we use predominantly the first parameter; however, for completeness we briefly look into the effect the width of the exciton has on the coupling; see the SI for details.

Figure 4 shows the optical spectra of a core−shell structure (r = 20 nm, $\hbar\gamma_{ex}$ = 50 meV) for increasing oscillator strengths from 0 to 0.5. As the oscillator strength increases, the splitting becomes greater and greater until it finally starts dominating over the plasmon damping, indicative of the strong coupling regime at about f > 0.05. Furthermore, one can clearly see the emergence of a third peak between the two modes to the blue and red of the plasmon resonance at f > 0.1. At first, the

dx.doi.org/10.1021/ph500032d | ACS Photonics 2014, 1, 454−463

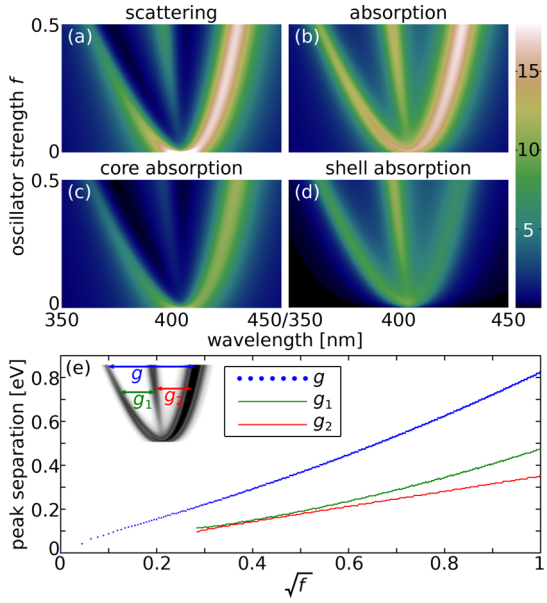

Figure 4. Optical properties of a core−shell structure with a silver core and the oscillator strength of the dye increasing from 0 to 0.5, r = 20 nm, $\hbar\gamma_{ex}$ = 50 meV. Efficiencies: (a) scattering, (b) absorption, (c) core absorption, (d) shell absorption. Note the two-peaked spectrum for small f and the appearance of the third peak at $f \approx 0.1$. (e) Peak separation (coupling strength equivalent) for the two high- and low-energy coupled peaks as well as their separation from the middle peak. Note the nearly linear dependence as a function of $\sqrt{f}$. The inset identifies splitting values g.

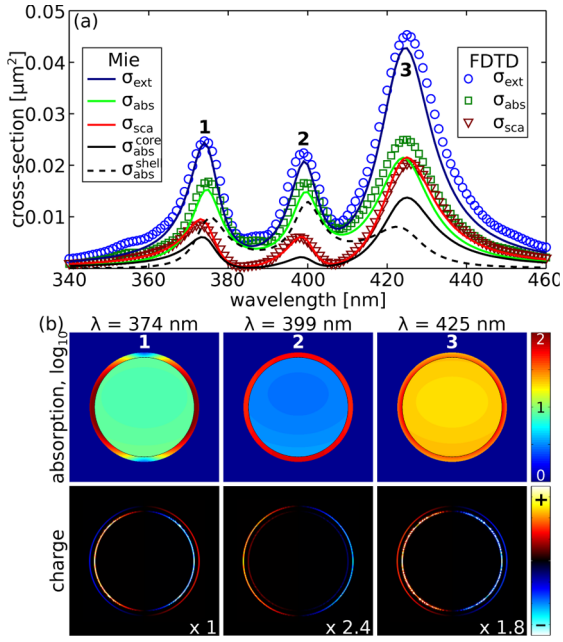

Figure 5. (a) Coupling of the plasmon and exciton in a core−shell nanostructure with a silver core and dye parameters $\hbar\gamma_{ex}$ = 50 meV, f = 0.3, h = 2 nm, and r = 20 nm gives a three-peaked spectrum in all cross sections. The FDTD and Mie spectra show excellent agreement. (b) For the three peaks marked in (a) we plot absorption and charge distributions for the above parameters, however, which are representative for any similar strongly coupled core−shell structure. In all cases absorption in the dye is enhanced considerably by the strong electric near-field of the plasmon. The distribution of surface charges for peaks 1 and 3 indicates those resonances are the bonding and antibonding combinations of the plasmon and exciton resonances. The middle peak, which has surface charges localized predominantly at the outer dye interface, is a collective mode that screens the metal core; this is also evident in a uniform electric field. The numbers indicate factors by which the amplitudes of surface charges were multiplied to use the same scale.

presence of this additional resonance is puzzling, since the coupling between two resonators characterized by an identical resonance frequency should give two new modes. However, the third mode is not an artifact and is confirmed by quasi-static as well as FDTD (see Figure 5) calculations. Additionally, in the SI in Figure S1 we present scattering and absorption spectra plotted as functions of wavelength and radius for increasing oscillator strengths to show the different behavior of the spectra.

Figure 4e shows splitting between various modes of the system as a function of the square root of the oscillator strength. All splitting follows nearly a linear relation with $\sqrt{f}$, in agreement with the well-known expression for the Rabi frequency, $g = \sqrt{N}\mu|E|$, taking into account that f scales linearly with N. Here, N is the number of molecules, μ is the molecular transition dipole moment, and $|E|$ is the electric field at the position of the molecule(s). This might seem rather surprising since the origin behind $\sqrt{N}$ lies in coherent oscillations of N dipoles, while Mie theory does not require any coherence but relies solely on dielectric response of the dye layer. Nevertheless, incorporation of dye permittivity into the core−shell structure produces a correct result, indicative of the applicability of classical electromagnetic approaches to this class of plasmon−exciton problems. Recalling the quasi-static analysis, the splitting between the eigenmodes $\tilde{\omega}_2 - \tilde{\omega}_1$ indeed scales approximately as $\sqrt{f}$.

To understand the nature of the resonances, we focus on one exemplary value of the oscillator strength (f = 0.3) for one core radius of 20 nm in Figure 5a. Here, we compare optical cross sections calculated using Mie theory and the FDTD method, which give very similar results. The three-peaked structure is visible in both absorption and scattering, as well as in both the core and shell absorption. This indicates that, indeed, the structure is strongly coupled, as can be expected for a large oscillator strength, strong field enhancement, and a large dye−metal volume ratio.

The coupling of the exciton to the plasmon is illustrated in Figure 5b with the distributions of absorption $\log_{10}(I(\varepsilon)|E|^2)$ and surface charges. The imaginary part of the dye permittivity at the left- and right-most peaks is relatively small, yet absorption at those wavelengths in the thin 2 nm shell is comparable to or greater than that in the core. The type of mode is clearly visualized by the polarization of the surface charges at the inner and outer interfaces. At the short wavelength (high-energy) peak interfaces located on the same side of the structure have opposite signs, while starting at the middle peak, they are the same. Thus, qualitatively the first resonance is different from the remaining ones. Despite a similar polarization of the interfaces, the middle and long wavelength peaks are considerably different. At 399 nm the charge is concentrated at the outer interface and the inner one is in comparison almost charge free. This is consistent with a uniform electric field in the particle (see Figure 6b and subsequent paragraphs for a discussion on electric fields) and suggests that the middle peak is qualitatively similar to a resonance of a homogeneous sphere. Finally, the long

dx.doi.org/10.1021/ph500032d | ACS Photonics 2014, 1, 454−463

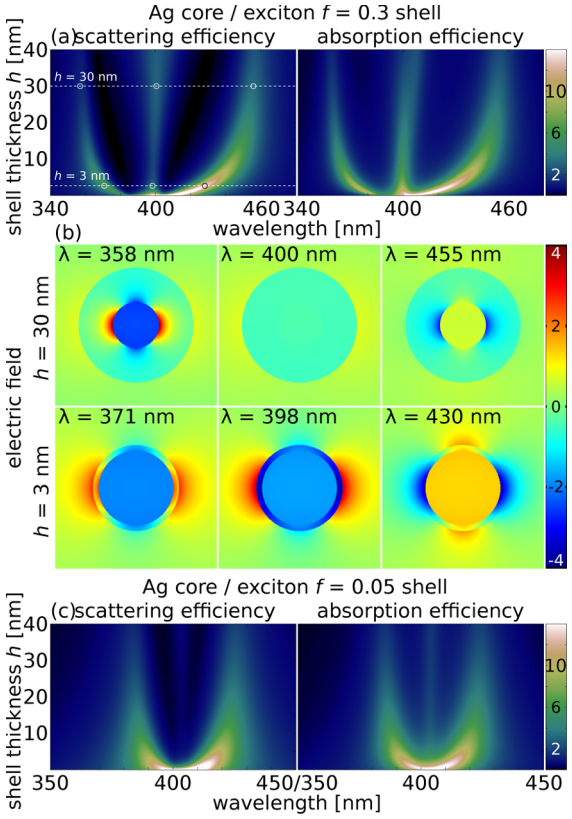

Figure 6. Scattering and absorption efficiencies for a core–shell structure (Ag core) as a function of h for r = 20 nm, $\hbar\gamma_{ex}$ = 50 meV, f = 0.3, and the exciton resonance is at the core resonance. (a) Plasmon–exciton coupling yields two modes above and below 400 nm with a separation that saturates for an increasing h. Additionally, a third mode at the exciton resonance is present. (b) The electric field plots show a core plasmon interacting with the exciton in the shell at the short- and long-wavelength modes (note the antiparallel fields in the core and shell). At the exciton resonance the third mode is characterized by an in-phase field distribution in the core and shell. (c) For f = 0.05 the splitting is weaker, but a weak third mode appears only for $h \geq 10$ nm. The larger h is, the larger the amount of dye that is weakly interacting with the plasmon and causes a background-like signal.

wavelength peak at λ = 425 nm shows strong surface charge densities at both interfaces, indicating strong coupling between the shell and the core, similar to that at λ = 374 nm. We note here that for a strongly coupled core–shell structure with a two-peaked spectrum the surface charge polarization of the peaks is the same as for the high- and low-energy resonances (peaks 1 and 3).

We further investigate the nature of the three modes, and in Figure 6 show the spectral dependence for an increasing shell thickness h that has f = 0.3. The three-peaked spectrum of the metal–dye structure is characterized by strong splitting of the outer two modes for small thicknesses and saturates at about 15 nm. This is expected, as the plasmon of the metal core has a short decay length and only weakly interacts with dye that is far away from the core–shell interface. The middle peak is virtually not affected by the scaling of the shell thickness, which is unexpected if the resonance is plasmon-like.

To understand the core–shell modes, it is necessary to look at the optical properties of Lorentz-material spheres and shells. Dye spheres and shells have for f < 1 one or two resonances,[45] respectively, although the second resonance for the shell appears when the real part of the permittivity becomes negative enough (see Figure S2). For the shell, one resonance remains at the exciton position (slight blue-shift) and the second weak one blue-shifts with increasing f. One resonance is a void mode, and the other is related to the exciton; moreover, these peaks shift only slightly when the shell thickness h increases (see Figure S3). When a shell is placed around a metal core such that $\omega_{sp} = \omega_{ex}$, the two shell modes interact with the plasmon resonance. This results in three coupled modes visible in scattering as well as both core and shell absorption. The coupled high- and low-energy modes are qualitatively identical to their equivalents for a two-peaked spectrum; however, the middle peak has a new character. Interestingly, the plot in Figure 6b for the middle peak reveals that the electric field is almost homogeneous, which would occur in a homogeneous sphere. Indeed, this is almost the case, as both the dye and core permittivities are negative. An important difference is that the magnitude of the dye's imaginary part is much larger than the core's, and expectedly absorption in the shell is dominant (cf. Figure 5). It is important to note that such a resonance can thus be observed only when the permittivity of the dye is negative enough, which is the onset of the second mode in a Lorentz shell. In our case this occurs at approximately f = 0.1, which is the threshold for the emergence of this third mode. An illustration of the pure dye core and shell resonances can be found in Figures S2 and S3.

Negative permittivity of a dye with a Lorentz dispersion relation is not the only condition that begets a three-peaked spectrum. Figure 6c presents scattering and absorption efficiencies of a core–shell structure with r = 20 nm and f = 0.05 for shell thicknesses $h \leq 40$ nm. In this case a weak peak at the exciton resonance is also observed, although it appears for $h \approx 10$ nm, a thickness greater than for f = 0.3 (Figure 6a). The middle peak for f = 0.05 is much more pronounced for absorption than scattering, similar to what happens for a dye shell, in contrast to Figure 6a, where they are of comparable amplitudes. This means that the nature of this resonance is different for f = 0.05 and 0.3. Indeed, the permittivity is always positive in the former case and a shell mode cannot be excited. Instead, there is a weakly polarized metal core (off resonance due to mode splitting) that enhances the electric field in the dye, resulting in enhanced absorption. Also, when the dye shell is thick enough it may act as a "background" medium for the core and the middle peak will be dominated by the spectrum of dye uncoupled to the core. For a comparison of the electric fields for f = 0.05 and 0.3 see Figure S4, while Figure S5 shows an exemplary plot detailing the split of absorption into core and shell contributions for a three-peaked spectrum for small f.

Avoided Crossing. By keeping one of the resonances at a constant wavelength and varying the second it is possible to obtain characteristic spectra that indicate the coupling regime. In Figure 7 we plot scattering and absorption spectra of a core–shell structure in which the core radius is constant, giving a fixed plasmon resonance, but the exciton resonance is varied from −100 to +100 nm relative to ω_{sp}. We perform this for the four distinct coupling regimes starting with enhanced absorption in Figure 7a,b (core radius 40 nm, f = 0.05). The scattering plot indicates coupling of the core and shell; however, the peak splitting is small. To demonstrate that the strong coupling regime is not achieved, we inspect the absorption spectrum. There a clear crossing of the plasmon and exciton is observed. For a larger field enhancement (r = 25 nm) the dip in scattering grows larger; however, the absorption

dx.doi.org/10.1021/ph500032d | ACS Photonics 2014, 1, 454–463

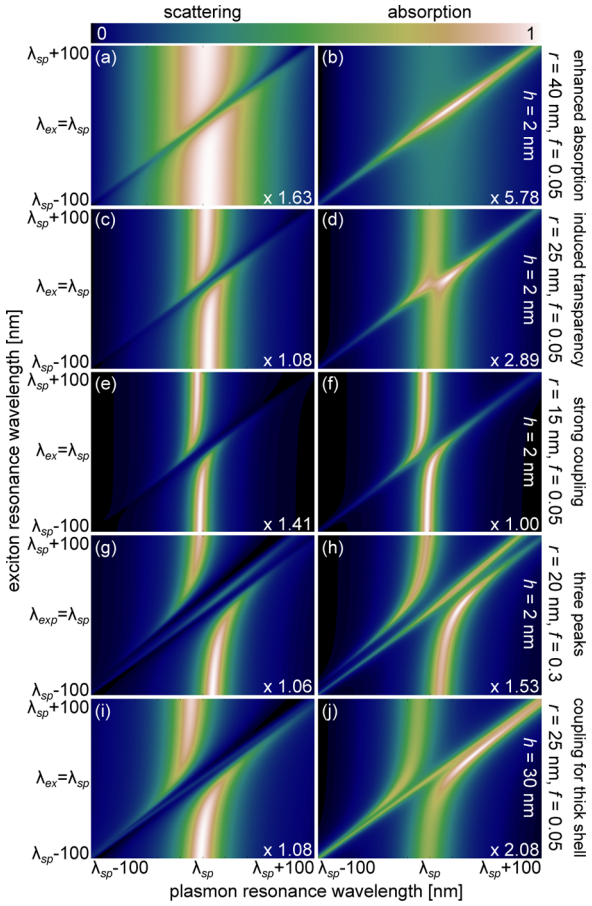

Figure 7. Emergence of anticrossing behavior in scattering and absorption for transition from (a, b) absorption enhancement via (c, d) induced transparency and (e, f) strong coupling to (g, h) three peaks. Anticrossing is observed in all cases for scattering; thus for complete analysis one also needs to investigate absorption spectra. For enhanced absorption the absorption spectra cross; for induced transparency the anticrossing behavior is very weak and only clearly appears for strong coupling. (i, j) For thick shells and low oscillator strength a three-peaked spectrum may be observed when the exciton and plasmon resonances overlap; however, the third mode exhibits crosses (joins) of the two coupled modes. The scaling factors indicate by how much individual spectra had to be multiplied to normalize their maximum values; that is, plot (f) displays the most intense spectrum.

plot still indicates a crossing behavior despite a small dip appearing at the center of the spectrum when the exciton and plasmon resonances match.

Definite anticrossing of both scattering and absorption is observed in Figure 7e,f when the radius is reduced to 15 nm, leading to an increase of the field enhancement. In this case the branches of scattering and absorption do not cross. The most interesting case occurs when the spectra are characterized by three peaks. The outermost plasmon/exciton branches avoid crossing; however, the third peak behavior is also interesting. Let us recall Figure S2, which shows the optical properties of a dye shell, which in addition to a peak at ω_{ex} exhibits an additional blue-shifted resonance, a void mode (cf. Figure S3b). When the plasmon and exciton resonances are far apart, those two dye modes are undisturbed and the spectrum shows the two of them either far to the blue or to the red of ω_{sp} (Figure 7g,h). When ω_{ex} tends to ω_{sp} from the blue side, the resonances couple and the dye void mode (the short-wavelength mode) turns to the plasmon resonance, while the plasmon turns into the bulk dye absorption peak. This means that the middle mode, which starts off at ω_{ex}, is converted into the void mode as the exciton resonance passes ω_{sp}.

Linking this three-peaked spectrum to the arrangement of the dye suggests that in a different geometry a three-peaked spectrum might not be observed for similar oscillator strengths. Indeed, Schlather et al.[23] in a dimer structure did not report it, although their Lorentz dispersion spanned a greater range of permittivities than for $f = 0.3$ in this work. On the other hand, Salomon et al. did observe the third peak for an increasing molecule density in a dye layer deposited on top of a grating.[6] To assess the influence of geometry on the spectra, we have conducted FDTD simulations for a dimer geometry (two silver ellipses with semiaxes of 60, 30, and 30 nm, a separation of 20 nm, and with a 40 nm dye sphere between them with the overlapping volume occupied by silver; results not shown) with the oscillator strength up to 3. It turns out that a very weak third peak (much weaker than in the dye-shell case) appears, although at much larger ($f \approx 0.6$) values than in the shell structure. This is connected with the fact that a dye core (here 20 nm in radius) exhibits a blue-shift of the optical resonances with increasing oscillator strengths and develops a second, very weak peak at the exciton resonance. Thus, a careful analysis of modes supported by the dye structure (no metal) is necessary to identify its inherent optical resonances, which then interact with the plasmon. This is consistent with the observation that a reduced dimensionality (a thin shell vs a sphere) gives rise to efficient coupling.[6] However, also very thick shells around a metal core exhibit a three-peaked spectrum, as shown in Figure 6, although the middle peak is not coupled to the other two.

This last case is illustrated in Figure 7i,j, in which we present optical spectra for a core−shell structure with a core radius of 25 nm, shell thickness of 30 nm, and oscillator strength $f = 0.05$. In scattering the avoided crossing is evident; however, the two coupled resonances are accompanied by a third weak one at $\lambda_{ex} = \lambda_{sp}$, where λ_{ex} and λ_{sp} are the exciton and plasmon resonance wavelengths, respectively. A similar situation occurs for absorption. The low- and high-energy peaks do not cross, but are joined (much stronger than for scattering) by a third absorption band. This clearly demonstrates that the third peak occurring for thick shells is simply a footprint of dye not coupled to the plasmon. Moreover, three peaks are present only when the exciton resonance is close in frequency to the plasmon; otherwise only two peaks are visible. This is in contrast to the strongly coupled three-peak case for $f = 0.3$.

Coupling to Metals with Interband Absorption. Up to this point we have been using a Drude model of silver for the core. However, a number of works make use of gold to support a plasmon. The significant difference between those two metals is a strong interband absorption regime in part of the optical range for Au with an onset just below 650 nm, while for Ag it starts below 350 nm. One outcome of this is a limit to the blue-shift of the plasmon resonance of Au nanoparticles due to shrinkage, where this limit is a consequence of damping losses. A similar process occurs when plasmon resonances hybridize and two new bonding and antibonding modes appear. Depending on the position of interband absorption either or both of these modes may be damped or shifted.[46,47]

Such mode damping and shifting may also be observed when a Drude−Lorentz metal is covered by a dye featuring an exciton at the surface plasmon resonance. In Figure 8 we show scattering and absorption efficiencies of a Drude−Lorentz core

dx.doi.org/10.1021/ph500032d | ACS Photonics 2014, 1, 454−463

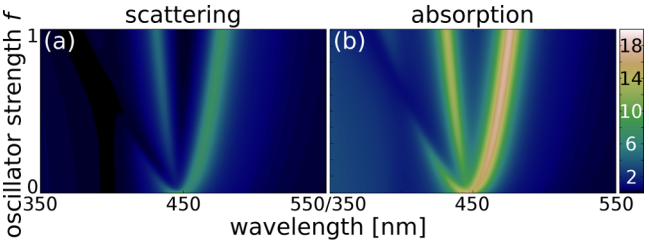

Figure 8. Three-peak strong coupling for a Drude−Lorentz metal core with scattering efficiencies (a) and absorption efficiencies (b). In comparison to a Drude metal core (see Figure 4a,b), interband absorption, i.e., the Lorentz contribution, causes a red-shift of the plasmon resonance and damping of the high-frequency coupled peak. As a result for large f only two peaks remain, but only one is a coupled plasmon−exciton resonance and the other is the shell mode.

(r = 20 nm) strongly coupled to a 2 nm dye layer with a variable oscillator strength and line width of $\hbar\gamma_{ex}$ = 50 meV. The Lorentz contribution that mimics interband absorption is arbitrarily chosen to resemble that of gold and be located to the blue of the plasmon resonance. Total permittivity is given by

$$\varepsilon_{DL}(\omega) = \varepsilon_p - \frac{{\omega_p}^2}{\omega(\omega + i\gamma)} + \sum_k \frac{\Delta_\varepsilon {\omega_k}^2}{{\omega_k}^2 - i\gamma_k\omega - \omega^2} \quad (8)$$

where Δ_ε = 0.05, $\hbar\gamma_k$ = 130 meV, and $\hbar\omega_k$ varies from 3.16 to 3.95 eV with 65.8 meV steps (in terms of angular frequency ω_k varies from 4800 Trad/s to 6000 Trad/s with 100 Trad/s steps). This extra dissipation makes a profound change in the scattering and absorption spectra.

The first change of the spectrum in relation to a Drude metal core is a red-shift of the plasmon resonance to 446 nm, at which we also set the exciton absorption line. For small oscillator strengths there is no qualitative change (cf. Figure 4a,b), and first two (f < 0.1) and then three peaks are present. The major difference is the rapid decay of the high-frequency mode, especially in scattering, which is the usual quantity to be measured. For f = 0.5 the scattering spectrum exhibits only two peaks, and when the exact nature of the two remaining resonances is not analyzed, strong coupling may be incorrectly identified. The reason for this is the fact that the middle mode is the dye-shell resonance that is not affected greatly by the plasmon. The strongly coupled modes are the left- and rightmost ones, and one of them is damped by the interband absorption. It is important to note, however, that an evaluation of the coupling strength based on the splitting of the two remaining modes will underestimate its value. Hence, the structure will be definitely in the strong coupling regime, as three peaks are observed for core−shell structures only in that regime. This is confirmed by optical spectra and distributions of the electric field, absorption, and surface charges for two cases with f = 0.3 (still three peaks visible) and 0.6 in Figure S6.

Finally, we would like to note that these observations are, in principle, equally applicable to both gold and silver. The key difference between these metals in the context of interband absorption is its onset: below ∼620 nm in Au vs below ∼320 nm in Ag. Its effect on LSPR spectra of gold nanoparticles is readily noticeable, and in order for the resonance to be moved away from it, either large particles, prolate or oblate in shape, or hollow shells made of gold have to employed. For silver nanoparticles the corresponding effect is less of an issue: the real part of permittivity of silver ($\mathrm{Re}(\varepsilon_{Ag})$) is −2 at about 350 nm, still above the onset of interband absorption, and $\mathrm{Re}(\varepsilon_{Ag})$ = −2 is the condition for the surface plasmon resonance of a sphere placed in a vacuum in the quasi-static approximation. Thus, we do not expect interband absorption to be as important a factor for silver as it is for gold. It should be mentioned that for such small particles other effects become important, namely, size quantization and surface screening, which may blue-shift the LSPR.[48] Thus, coupling between very small Ag nanoparticles and molecules will be affected by interband absorption, although such investigations require tools such as time-dependent density functional theory and are outside the scope of the present work.

CONCLUSIONS

In conclusion, we have studied plasmon−exciton interaction in a spherical core−shell geometry as a function of geometrical parameters and oscillator strength of the shell layer (for a brief discussion on the effect of the line width see Figure S7 and the accompanying discussion). We have shown that scattering spectra under the investigated parameter range always comprise dips at the exciton resonance. However, the absorption cross-section may have both peaks and dips depending on the particle size and the oscillator strength. Furthermore, we have decomposed the absorption into core and shell contributions and shown that the core absorption always has a dip as a result of shell screening, while the shell contribution may vary between a peak-like and a dip-like behavior. On the basis of these results we classify interaction regimes as enhanced absorption (peak in total absorption), induced transparency (dip in total absorption but splitting weaker than plasmon width), and strong coupling (splitting larger than plasmon width in both scattering and absorption). We show that to confidently assign the interaction regime, it is more instructive to follow mode anticrossing in absorption rather than in scattering, as the latter shows anticrossing even for the enhanced-absorption case. It is important to note, however, that the difference between enhanced-absorption and induced-transparency regimes is determined not only by the oscillator strength but also by the width of exciton transition γ_{ex}. A smaller particle and a higher oscillator strength of the shell lead to stronger coupling, in agreement with the well-known scaling for the vacuum Rabi splitting that is proportional to the field enhancement and square root of the number of molecules (oscillator strength). Moreover, at high oscillator strength, when the permittivity of the dye reaches negative values, we observe the emergence of three peaks in both scattering and absorption, a scenario strongly deviating from a simplified coupled harmonic oscillator analogy. On the basis of field and charge distribution around the nanostructures, we assign those peaks to strong coupling and geometrical resonance of the system as a whole. This is further confirmed by the mode anticrossing behavior seen for the three-peaked spectra. Finally, we should point out that classical electrodynamics methods presented in this study give an adequate description of the static optical properties of core−shell structures, and in general good agreement between our results and previously reported experimental[8,10,14,17,19] and theoretical[1,5] observations is found; however, when it comes to dynamic properties, such as ultrafast oscillations, beats, and revivals, as well as saturation effects, fully quantum mechanical or quantum optics approaches are more appropriate.[4,7,41]

dx.doi.org/10.1021/ph500032d | ACS Photonics 2014, 1, 454−463

■ ASSOCIATED CONTENT

Supporting Information

Full derivation of the quasi-static analysis, additional optical spectra of the considered structure, as well as complementary structures to support drawn conclusions, including Figures S1–S7. This material is available free of charge via the Internet at http://pubs.acs.org.

■ AUTHOR INFORMATION

Corresponding Authors

*E-mail: tomasz.antosiewicz@uw.edu.pl.
*E-mail: timurs@chalmers.se.

Notes

The authors declare no competing financial interest.

■ ACKNOWLEDGMENTS

This work was supported by the Foundation for Polish Science via the project HOMING PLUS/2013-7/1, the Swedish Foundation for Strategic Research, Swedish Research Council (VR), Knut and Alice Wallenberg Foundation, and Chalmers Area of Advance (Nanoscience and Nanotechnology).

■ REFERENCES

(1) Ambjörnsson, T.; Mukhopadhyay, G.; Apell, S. P.; Käll, M. Resonant coupling between localized plasmons and anisotropic molecular coatings in ellipsoidal metal nanoparticles. *Phys. Rev. B* **2006**, *73*, 085412.

(2) Wu, X.; Gray, S. K.; Pelton, M. Quantum-dot-induced transparency in a nanoscale plasmonic resonator. *Opt. Express* **2010**, *18*, 23633–23645.

(3) Savasta, S.; Saija, R.; Ridolfo, A.; Di Stefano, O.; Denti, P.; Borghese, F. Nanopolaritons: vacuum Rabi splitting with a single quantum dot in the center of a dimer nanoantenna. *ACS Nano* **2010**, *4*, 6369–6376.

(4) Manjavacas, A.; Abajo, F. J. G. d.; Nordlander, P. Quantum plexcitonics: strongly interacting plasmons and excitons. *Nano Lett.* **2011**, *11*, 2318–2323.

(5) Chen, H.; Shao, L.; Woo, K. C.; Wang, J.; Lin, H.-Q. Plasmonic-molecular resonance coupling: plasmonic splitting versus energy transfer. *J. Phys. Chem. C* **2012**, *116*, 14088–14095.

(6) Salomon, A.; Gordon, R. J.; Prior, Y.; Seideman, T.; Sukharev, M. Strong coupling between molecular excited states and surface plasmon modes of a slit array in a thin metal film. *Phys. Rev. Lett.* **2012**, *109*, 073002.

(7) Chen, X.-W.; Sandoghdar, V.; Agio, M. Coherent interaction of light with a metallic structure coupled to a single quantum emitter: from superabsorption to cloaking. *Phys. Rev. Lett.* **2013**, *110*, 153605.

(8) Zengin, G.; Johansson, G.; Johansson, P.; Antosiewicz, T. J.; Käll, M.; Shegai, T. Approaching the strong coupling limit in single plasmonic nanorods interacting with J-aggregates. *Sci. Rep.* **2013**, *3*, 3074.

(9) Bellessa, J.; Bonnand, C.; Plenet, J. C.; Mugnier, J. Strong coupling between surface plasmons and excitons in an organic semiconductor. *Phys. Rev. Lett.* **2004**, *93*, 036404.

(10) Wiederrecht, G. P.; Wurtz, G. A.; Hranisavljevic, J. Coherent coupling of molecular excitons to electronic polarizations of noble metal nanoparticles. *Nano Lett.* **2004**, *4*, 2121–2125.

(11) Dintinger, J.; Klein, S.; Bustos, F.; Barnes, W. L.; Ebbesen, T. W. Strong coupling between surface plasmon-polaritons and organic molecules in subwavelength hole arrays. *Phys. Rev. B* **2005**, *71*, 035424.

(12) Uwada, T.; Toyota, R.; Masuhara, H.; Asahi, T. Single particle spectroscopic investigation on the interaction between exciton transition of cyanine dye J-aggregates and localized surface plasmon polarization of gold nanoparticles. *J. Phys. Chem. C* **2007**, *111*, 1549–1552.

(13) Wurtz, G. A.; Evans, P. R.; Hendren, W.; Atkinson, R.; Dickson, W.; Pollard, R. J.; Zayats, A. V. Molecular plasmonics with tunable exciton-plasmon coupling strength in J-aggregate hybridized Au nanorod assemblies. *Nano Lett.* **2007**, *7*, 1297–1303.

(14) Liu, G. L.; Long, Y.-T.; Choi, Y.; Kang, T.; Lee, L. P. Quantized plasmon quenching dips nanospectroscopy via plasmon resonance energy transfer. *Nat. Methods* **2007**, *4*, 1015–1017.

(15) Fofang, N. T.; Park, T.-H.; Neumann, O.; Mirin, N. A.; Nordlander, P.; Halas, N. J. Plexcitonic nanoparticles: plasmon-exciton coupling in nanoshell-J-aggregate complexes. *Nano Lett.* **2008**, *8*, 3481–3487.

(16) Bellessa, J.; Symonds, C.; Vynck, K.; Lemaitre, A.; Brioude, A.; Beaur, L.; Plenet, J. C.; Viste, P.; Felbacq, D.; Cambril, E.; Valvin, P. Giant Rabi splitting between localized mixed plasmon-exciton states in a two-dimensional array of nanosize metallic disks in an organic semiconductor. *Phys. Rev. B* **2009**, *80*, 033303.

(17) Ni, W.; Ambjönsson, T.; Apell, S. P.; Chen, H.; Wang, J. Observing plasmonic-molecular resonance coupling on single gold nanorods. *Nano Lett.* **2010**, *10*, 77–84.

(18) Zheng, Y. B.; Juluri, B. K.; Lin Jensen, L.; Ahmed, D.; Lu, M.; Jensen, L.; Huang, T. J. Dynamic tuning of plasmon–exciton coupling in arrays of nanodisk–J-aggregate complexes. *Adv. Mater.* **2010**, *22*, 3603–3607.

(19) Djoumessi Lekeufack, D.; Brioude, A.; Coleman, A. W.; Miele, P.; Bellessa, J.; De Zeng, L.; Stadelmann, P. Core-shell gold J-aggregate nanoparticles for highly efficient strong coupling applications. *Appl. Phys. Lett.* **2010**, *96*, 253107.

(20) Fofang, N. T.; Grady, N. K.; Fan, Z.; Govorov, A. O.; Halas, N. J. Plexciton dynamics: exciton-plasmon coupling in a J-aggregate-Au nanoshell complex provides a mechanism for nonlinearity. *Nano Lett.* **2011**, *11*, 1556–1560.

(21) Schwartz, T.; Hutchison, J. A.; Genet, C.; Ebbesen, T. W. Reversible switching of ultrastrong light-molecule coupling. *Phys. Rev. Lett.* **2011**, *106*, 196405.

(22) Hutchison, J. A.; Schwartz, T.; Genet, C.; Devaux, E.; Ebbesen, T. W. Modifying chemical landscapes by coupling to vacuum fields. *Angew. Chem., Int. Ed.* **2012**, *51*, 1592–1596.

(23) Schlather, A. E.; Large, N.; Urban, A. S.; Nordlander, P.; Halas, N. J. Near-field mediated plexitonic coupling and giant Rabi splitting in individual metallic dimers. *Nano Lett.* **2013**, *13*, 3281–3286.

(24) Vasa, P.; Wang, W.; Pomraenke, R.; Lammers, M.; Maiuri, M.; Manzoni, C.; Cerullo, G.; Lienau, C. Real-time observation of ultrafast Rabi oscillations between excitons and plasmons in metal nanostructures with J-aggregates. *Nat. Photonics* **2013**, *7*, 128–132.

(25) Margapoti, E.; Gentili, D.; Amelia, M.; Credi, A.; Morandi, V.; Cavallini, M. Tailoring of quantum dot emission efficiency by localized surface plasmon polaritons in self-organized mesoscopic rings. *Nanoscale* **2014**, *6*, 741–744.

(26) Thompson, R. J.; Rempe, G.; Kimble, H. J. Observation of normal-mode splitting for an atom in an optical cavity. *Phys. Rev. Lett.* **1992**, *68*, 1132–1135.

(27) Yoshie, T.; Scherer, A.; Hendrickson, J.; Khitrova, G.; Gibbs, H. M.; Rupper, G.; Ell, C.; Shchekin, O. B.; Deppe, D. G. Vacuum Rabi splitting with a single quantum dot in a photonic crystal nanocavity. *Nature* **2004**, *432*, 200–203.

(28) Aoki, T.; Dayan, B.; Wilcut, E.; Bowen, W. P.; Parkins, A. S.; Kippenberg, T. J.; Vahala, K. J.; Kimble, H. J. Observation of strong coupling between one atom and a monolithic microresonator. *Nature* **2006**, *443*, 671–674.

(29) Jeanmaire, D. L.; Van Duyne, R. P. Surface Raman spectroelectrochemistry. *J. Electroanal. Chem.* **1977**, *84*, 1–20.

(30) Kneipp, K.; Wang, Y.; Kneipp, H.; Perelman, L. T.; Itzkan, I.; Dasari, R. R.; Feld, M. S. Single molecule detection using surface-enhanced Raman scattering (SERS). *Phys. Rev. Lett.* **1997**, *78*, 1667–1670.

(31) Nie, S.; Emory, S. R. Probing single molecules and single nanoparticles by surface-enhanced Raman scattering. *Science* **1997**, *275*, 1102–1106.

(32) Xu, H.; Bjerneld, E. J.; Käll, M.; Börjesson, L. Spectroscopy of single hemoglobin molecules by surface enhanced Raman scattering. *Phys. Rev. Lett.* **1999**, *83*, 4357−4360.
(33) Shegai, T.; Li, Z.; Dadosh, T.; Zhang, Z.; Xu, H.; Haran, G. Managing light polarization via polasmon-molecule interactions within an asymmetric metal nanoparticle trimer. *Proc. Natl. Acad. Sci. U.S.A.* **2008**, *105*, 16448−16453.
(34) Neubrech, F.; Pucci, A.; Cornelius, T. W.; Karim, S.; García-Etxarri, A.; Aizpurua, J. Resonant plasmonic and vibrational coupling in a tailored nanoantenna for infrared detection. *Phys. Rev. Lett.* **2008**, *101*, 157403.
(35) Anger, P.; Bharadwaj, P.; Novotny, L. Enhancement and Quenching of Single-Molecule Fluorescence. *Phys. Rev. Lett.* **2006**, *96*, 113002.
(36) Frontiera, R. R.; Gruenke, N. L.; Van Duyne, R. P. Fano-like resonances arising from long-lived molecule-plasmon interactions in colloidal nanoantennas. *Nano Lett.* **2012**, *12*, 5989−5994.
(37) Zamecnik, C. R.; Ahmed, A.; Walters, C. M.; Gordon, R.; Walker, G. C. Surface-enhanced Raman spectroscopy using lipid encapsulated plasmonic nanoparticles and J-aggregates to create locally enhanced electric fields. *J. Phys. Chem. C* **2013**, *117*, 1879−1886.
(38) Jin, S.; Son, H.-J.; Farha, O. K.; Wiederrecht, G. P.; Hupp, J. T. Energy transfer from quantum dots to metal-organic frameworks for enhanced light harvesting. *J. Am. Chem. Soc.* **2013**, *135*, 955−958.
(39) Son, H.-J.; Jin, S.; Patwardhan, S.; Wezenberg, S. J.; Jeong, N. C.; So, M.; Wilmer, C. E.; Sarjeant, A. A.; Schatz, G. C.; Snurr, R. Q.; Farha, O. K.; Wiederrecht, G. P.; Hupp, J. T. Light-harvesting and ultrafast energy migration in poryphin-based-metal-organic frameworks. *J. Am. Chem. Soc.* **2013**, *135*, 826−869.
(40) Lee, J.; Hernandez, P.; Lee, J.; Govorov, A. O.; Kotov, N. A. Exciton-plasmon interactions in molecular spring assemblies of nanowires and wavelength-based protein detection. *Nat. Mater.* **2007**, *6*, 291−295.
(41) Shah, R. A.; Scherer, N. F.; Pelton, M.; Gray, S. K. Ultrafast reversal of a Fano resonance in a plasmon-exciton system. *Phys. Rev. B* **2013**, *88*, 075411.
(42) Johnson, P.; Christy, R. Optical constants of the noble metals. *Phys. Rev. B* **1972**, *6*, 4370−4379.
(43) Antosiewicz, T. J.; Szoplik, T. Corrugated metal-coated tapered tip for scanning near-field optical microscope. *Opt. Express* **2007**, *15*, 10920−10928.
(44) Bohren, C.; Huffman, D. *Absorption and Scattering of Light by Small Particles*; John Wiley and Sons, Inc.: New York, 1983.
(45) Gülen, D. Optical response of Lorentzian nanoshells in the quasistatic limit. *J. Phys. Chem. B* **2013**, *117*, 11220−11228.
(46) Pakizeh, T. Optical absorption of plasmonic nanoparticles in presence of a local interband transition. *J. Phys. Chem. C* **2011**, *115*, 21826−21831.
(47) Schwind, M.; Kasemo, B.; Zorić, I. Localized and propagating plasmons in metan films with nanoholes. *Nano Lett.* **2013**, *13*, 1743−1750.
(48) Monreal, R. C.; Antosiewicz, T. J.; Apell, S. P. Competition between surface screening and size quantization for surface plasmons in nanoparticles. *New J. Phys.* **2013**, *15*, 083044.